Electric field control of magnetic susceptibility in laminate magnetostrictive/piezoelectric composites: Phase-field simulation and theoretical model

Liwei D. Geng,[1] Yongke Yan,[2] Shashank Priya,[2] and Yu U. Wang[1,*]

[1]*Department of Materials Science and Engineering, Michigan Technological University, Houghton, Michigan 49931, USA*

[2]*Department of Materials Science and Engineering, Pennsylvania State University, University Park, Pennsylvania 16802, USA*

(Received 29 August 2019; accepted 30 January 2020; published 18 February 2020)

Electric field control of magnetic susceptibility in laminate magnetostrictive/piezoelectric composites promises to create a new class of magnetoelectric elements, voltage tunable inductors. To elucidate the underlying mechanism of electric field modulated magnetic susceptibility at the domain level, phase-field modeling, and computer simulation are employed to systematically study the laminate magnetoelectric composites of Terfenol-D and PZT, where polycrystalline Terfenol-D can provide a giant magnetoelectric coupling that is important for high-tunability voltage tunable inductors. The simulations focus on the interplay between magnetocrystalline anisotropy and stress-induced anisotropy that is induced by electric field and reveal three regimes of magnetic susceptibility behaviors: constant (regime I), fast-varying (regime II), and reciprocal linear (regime III), where regimes II and III can give rise to a high tunability. Such three regimes are attributed to different magnetization distribution and evolution mechanisms that are modulated by the stress-induced anisotropy. To further characterize the electric field control of magnetic susceptibility behaviors, a general theoretical model of laminate magnetoelectric (ME) composites based on polycrystalline magnetostrictive materials is developed, which reproduces the three regimes of susceptibility behaviors for polycrystalline Terfenol-D material. The general theoretical model for this specific system can also be extended to other laminate polycrystalline ME composites.

DOI: 10.1103/PhysRevB.101.054422

I. INTRODUCTION

Magnetoelectric (ME) coupling effect that arises from the cross-linking between magnetostrictive and piezoelectric properties via the interface in multiferroic materials is of fundamental and technical importance in creating novel electronic and spintronic devices [1–5]. While the direct ME effect (the appearance of an electric polarization upon applying a magnetic field) has been extensively studied [6–14], the converse ME effect, especially the modulation of magnetic susceptibility or permeability by electric field, was much less investigated. In particular, multiferroic laminate composites made of magnetostrictive and piezoelectric phases take advantage of strain-mediated interaction that allows control of magnetic susceptibility or permeability through electric field or voltage via the converse ME coupling effect, and promise to develop a new class of ME components, voltage tunable inductors (VTIs) [15–18], which is very important for enhancing the efficiency of power electronics as well as reducing the number of passives by actively changing the magnitude of inductance. Thus, an understanding of electric field control of magnetic susceptibility in laminate ME composites at the domain level and even further, from a phenomenological theoretical model, is required.

Bichurin, Petrov, and Srinivasan have developed various phenomenological theoretical models to elucidate the ME coupling mechanisms in laminate magnetostrictive/piezoelectric composites of various forms and conditions [11–14]. While most of those theoretical works were related to the direct ME effect, the theoretical model for electric field control of magnetic susceptibility in laminate ME composites is still lacking. Through the strain-mediated interaction, applying an electric field on the piezoelectric layer can exert a stress on the magnetostrictive layer, and thus, it is actually the interplay between magnetocrystalline anisotropy and stress-induced anisotropy of the magnetostrictive layer that determines the susceptibility behaviors modulated by electric field, which means that susceptibility behaviors exhibited by different magnetostrictive materials must be different due to their different magnetocrystalline anisotropies. However, since polycrystalline magnetostrictive materials are more commonly used in ME composites, whose grain orientations are randomly distributed, the effect of individual magnetocrystalline anisotropy could be "averaged" in a certain manner so as to exhibit a more general effective magnetic anisotropy eventually, which allows the existence of a general behavior of magnetic susceptibility modulated by electric field. Thus, we will develop a theoretical model to describe this general behavior.

Among various magnetostrictive materials, Terfenol-D, a rare-earth-iron alloy, is the most widely used giant magnetostrictive alloy that exhibits a very high magnetostriction (over 1000 ppm) as well as a large magnetocrystalline anisotropy, and the composites made of Terfenol-D and piezoelectric materials can manifest a strong ME coupling effect. Such a giant ME coupling as well as the underlying

*Author to whom correspondence should be addressed: wangyu@mtu.edu

mechanism was discussed in detail by Nan *et al.* in a review on Terfenol-D-based ME composites [2]. Since a giant ME coupling usually leads to a large tunability of magnetic susceptibility that is an essential factor of VTIs, we adopt polycrystalline Terfenol-D as the magnetostrictive material for our laminate ME composite system in this work to systematically study the electric field control of magnetic susceptibility behaviors by employing domain-level phase-field modeling and computer simulation. The simulations focus on the interplay between magnetocrystalline anisotropy and stress-induced anisotropy. Such a stress-induced anisotropy is mainly introduced by two types of strain, namely, electric field tunable strain and internal bias strain. The simulations reveal three regimes of susceptibility, which are further characterized by a theoretical model developed for laminate ME composite systems and good agreement is obtained. Such a general theoretical model can be also extended to other laminate ME composites, for example, similar susceptibility or permeability behaviors were also observed in our recent experimental studies of cofired [19] and bonded [18] polycrystalline ferrite/$Pb(Mg_{1/3}Nb_{2/3})O_3$-$PbTiO_3$ (PMN-PT) ME composites. In fact, because of the polycrystalline microstructure of Terfenol-D, this work exhibits a different magnetization evolution mechanism and thus a different magnetic susceptibility behavior from the previous amorphous Metglas/PZT model system [20] which does not exhibit the polycrystalline nature and hence significantly reduces the complexity to develop a theoretical model.

II. PHASE-FIELD MODELING

In ME composites consisting of magnetostrictive and ferroelectric phases, the evolution of magnetic and electric domains is coupled with their secondary elastic domains due to magnetostriction and electrostriction. The phase-field ME composite model integrates two stand-alone phase-field models for magnetostrictive materials [21] and ferroelectric materials [22] that are developed in our previous works, which treats domain processes, grain structures, and phase morphology in two-phase polycrystalline composites. This model allows the strain-mediated domain-level coupling between magnetization and polarization, and the electrical conductivity in magnetostrictive phase is also considered. While this section will only briefly describe this ME composite model, more detailed description can be found in our previous publications [20,23].

The state of a ME composite can be described by fields of magnetization $\mathbf{M}(\mathbf{r})$, polarization $\mathbf{P}(\mathbf{r})$, and free charge density $\rho(\mathbf{r})$. The total system free energy under externally applied magnetic field $\mathbf{H}^{\text{ex}}$ and electric field $\mathbf{E}^{\text{ex}}$ is [21,22]

$$F = \int [(1-\eta) f_{\text{M}}(R_{ij}M_j) + \eta f_{\text{E}}(R_{ij}P_j) + \beta_{\text{M}}|\nabla \mathbf{M}|^2 + \beta_{\text{E}}|\nabla \mathbf{P}|^2 - \mu_0 \mathbf{H}^{\text{ex}} \cdot \mathbf{M} - \mathbf{E}^{\text{ex}} \cdot \mathbf{P}] d^3 r + \int \frac{d^3k}{(2\pi)^3} \left[\frac{\mu_0}{2} |\mathbf{n} \cdot \tilde{\mathbf{M}}|^2 + \frac{1}{2\varepsilon_0} \left| \frac{\tilde{\rho}}{k} - i\mathbf{n} \cdot \tilde{\mathbf{P}} \right|^2 + \frac{1}{2} K_{ijkl} \tilde{\varepsilon}_{ij} \tilde{\varepsilon}^*_{kl} \right], \quad (1)$$

where $f_{\text{M}}(R_{ij}M_j)$ and $f_{\text{E}}(R_{ij}P_j)$ are the local free-energy density of magnetostrictive and ferroelectric phases, respectively. Both $\mathbf{M}(\mathbf{r})$ and $\mathbf{P}(\mathbf{r})$ are defined in a global coordinate system of the composite. The operations $R_{ij}M_j$ and $R_{ij}P_j$ in the functions $f_{\text{M}}(R_{ij}M_j)$ and $f_{\text{E}}(R_{ij}P_j)$ transform $\mathbf{M}(\mathbf{r})$ and $\mathbf{P}(\mathbf{r})$ from the global system to the local crystallographic system in each grain. Figure 1 shows the grain structure of the two-phase ME composite used in our simulations, where the two-phase morphology of the composite is characterized by a phase-field variable $\eta(\mathbf{r})$ that distinguishes magnetostrictive grains ($\eta = 0$) and ferroelectric grains ($\eta = 1$). In the local crystallographic system, $f_{\text{M}}(\mathbf{M})$ is formulated as the magnetocrystalline anisotropy energy [24]:

$$f_{\text{M}}(\mathbf{M}) = K_1 \left(m_1^2 m_2^2 + m_2^2 m_3^2 + m_3^2 m_1^2 \right) + K_2 m_1^2 m_2^2 m_3^2, \quad (2)$$

where $\mathbf{m} = \mathbf{M}/M$ is the magnetization direction, K_1 and K_2 are the magnetic anisotropy constants, and $f_{\text{E}}(\mathbf{P})$ is formulated by the Landau-Ginzburg-Devonshire (LGD) polynomial energy [25]:

$$f_{\text{E}}(\mathbf{P}) = \alpha_1 \left(P_1^2 + P_2^2 + P_3^2 \right) + \alpha_{11} \left(P_1^4 + P_2^4 + P_3^4 \right) + \alpha_{12} \left(P_1^2 P_2^2 + P_2^2 P_3^2 + P_3^2 P_1^2 \right) + \alpha_{111} \left(P_1^6 + P_2^6 + P_3^6 \right) + \alpha_{112} \left[P_1^4 \left(P_2^2 + P_3^2 \right) + P_2^4 \left(P_3^2 + P_1^2 \right) + P_3^4 \left(P_1^2 + P_2^2 \right) \right] + \alpha_{123} P_1^2 P_2^2 P_3^2, \quad (3)$$

where α's are the expansion coefficients. The two gradient terms in Eq. (1) characterize the energy contributions from the magnetization gradient (exchange energy) and polarization gradient, respectively. The $\mathbf{k}$-space integral terms characterize the domain configuration-dependent energies of the long-range magnetostatic, electrostatic, and elastostatic interactions, where $\tilde{\mathbf{M}}(\mathbf{k})$, $\tilde{\mathbf{P}}(\mathbf{k})$, $\tilde{\rho}(\mathbf{k})$, and $\tilde{\varepsilon}(\mathbf{k})$ are the Fourier transforms of the respective field variables $\mathbf{M}(\mathbf{r})$, $\mathbf{P}(\mathbf{r})$, $\rho(\mathbf{r})$, and $\varepsilon(\mathbf{r})$, $K_{ijkl} = C_{ijkl} - n_m C_{ijmn} \Omega_{np} C_{klpq} n_q$, $\Omega_{ik} = (C_{ijkl} n_j n_l)^{-1}$, C_{ijkl} is the elastic stiffness tensor, and $\mathbf{n} = \mathbf{k}/k$. The spontaneous strain ε results from magnetostriction and electrostriction, $\varepsilon_{ij} = \lambda_{ijkl} m_k m_l + Q_{ijkl} P_k P_l$, where λ_{ijkl} and Q_{ijkl} are magnetostrictive and electrostrictive coefficient tensors, respectively.

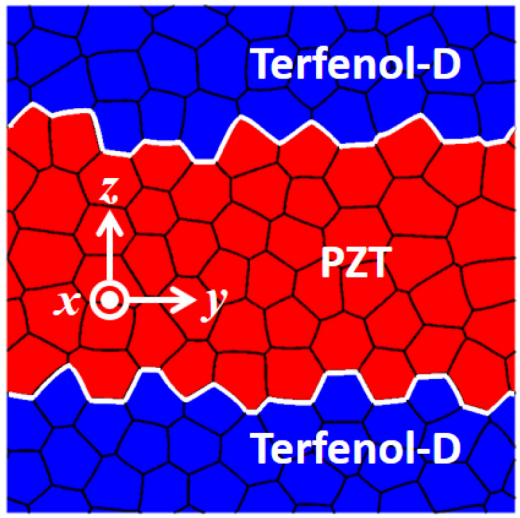

FIG. 1. Grain structure and phase morphology of laminate ME composite. Blue color represents magnetostrictive phase and red color represents piezoelectric phase.

The domain evolution described by magnetization $\mathbf{M}(\mathbf{r},t)$ and polarization $\mathbf{P}(\mathbf{r},t)$ are, respectively, governed by the Landau-Lifshitz-Gilbert equation [26] and the time-dependent Ginzburg-Landau equation [27]:

$$\frac{\partial \mathbf{M}(\mathbf{r},t)}{\partial t} = \gamma\, \mathbf{M} \times \frac{\delta F}{\delta \mathbf{M}(\mathbf{r},t)} + \alpha\, \mathbf{M} \times \left[\mathbf{M} \times \frac{\delta F}{\delta \mathbf{M}(\mathbf{r},t)}\right], \tag{4}$$

$$\frac{\partial \mathbf{P}(\mathbf{r},t)}{\partial t} = -L\frac{\delta F}{\delta \mathbf{P}(\mathbf{r},t)}, \tag{5}$$

where γ and α are gyromagnetic ratio and damping parameter, respectively, for magnetization evolution, and L is kinetic coefficient for polarization evolution. The evolution of free charge density field $\rho(\mathbf{r},t)$ is governed by charge conservation and microscopic Ohm's law [28]:

$$\frac{\partial \rho(\mathbf{r},t)}{\partial t} = -\nabla \cdot \mathbf{j}(\mathbf{r},t), \tag{6}$$

$$j_i = \sigma_{ik} E_k, \tag{7}$$

where $\sigma_{ik}(\mathbf{r})$ is the electrical conductivity distribution in the ME composite. The local electric field $\mathbf{E}(\mathbf{r})$ that is generated by free charge density distribution $\rho(\mathbf{r})$ and polarization distribution $\mathbf{P}(\mathbf{r})$ as well as externally applied electric field $\mathbf{E}^{\text{ex}}$ is given by

$$\mathbf{E}(\mathbf{r}) = \mathbf{E}^{\text{ex}} - \frac{1}{\varepsilon_0}\int \frac{d^3k}{(2\pi)^3}\left[\mathbf{n}\cdot\tilde{\mathbf{P}}(\mathbf{k}) + i\frac{\tilde{\rho}(\mathbf{k})}{k}\right]\mathbf{n}e^{i\mathbf{k}\cdot\mathbf{r}}. \tag{8}$$

In this computational study of laminate ME composites, $Tb_xDy_{1-x}Fe_2$ (Terfenol-D) [24] and $Pb(Zr_{1-x}Ti_x)O_3$ (PZT) [25] are considered as model magnetostrictive and ferroelectric materials. The material-specific input parameters used in this work are magnetocrystalline anisotropy constants $K_1 = -6\times10^4$ J/m^3, $K_2 = -2\times10^5$ J/m^3, saturation magnetization $M_s = 8\times10^5$ A/m, magnetostrictive constants $\lambda_{111} = 1.64\times10^{-3}$, $\lambda_{100} = 1\times10^{-4}$ for Terfenol-D [24]; and LGD coefficients $\alpha_1 = -2.67\times10^7$ m/F, $\alpha_{11} = -1.43\times10^7$ m^5/C^{2}F, $\alpha_{12} = 1.57\times10^7$ m^5/C^{2}F, $\alpha_{111} = 1.34\times10^8$ m^9/C^{4}F, $\alpha_{112} = 1.17\times10^9$ m^9/C^{4}F, $\alpha_{123} = -4.77\times10^9$ m^9/C^{4}F, electrostrictive constants $Q_{11} = 0.0966$ m^4/C^2, $Q_{12} = -0.046$ m^4/C^2, $Q_{44} = 0.0819$ m^4/C^2 for $Pb(Zr_{0.5}Ti_{0.5})O_3$ [25,29]. While these material-specific parameters are used in this work, the obtained simulation results reflect general behaviors of laminate ME composite made of polycrystalline magnetostrictive and piezoelectric materials.

III. SIMULATION RESULTS AND DISCUSSION

In this computational study, we focus on the interplay between magnetocrystalline anisotropy and stress-induced anisotropy on laminate Terfenol-D/PZT ME composites. Such a stress-induced anisotropy is mainly introduced by two types of strain, namely, electric field tunable strain and internal bias strain. The electric field tunable strain is induced by electric field. When the electric field is applied perpendicular to the PZT layer (i.e., along the z axis), a compressive strain will be transferred to the magnetostrictive Terfenol-D layer and exert a compressive stress on it due to the strain coupling. Such a compressive stress can induce an effective uniaxial magnetic anisotropy on Terfenol-D layer, i.e., the stress-induced anisotropy, to control its magnetic properties. Unlike the electric field tunable strain, the internal bias strain introduced by specific means does not change with the tunable electric field, so the resultant stress-induced anisotropy is constant and independent of the electric field.

Although internal bias strain can be introduced in different ways, two types of bias strain commonly exist in ME composites, namely, the preexisting strain and the thermal mismatch strain. The preexisting strain can be caused by electrically poling the piezoelectric layer, while the thermal mismatch strain that usually exists in cofired laminate composites arises from different thermal expansion coefficients of the layers of different phases. These two types of bias strain produce similar effect on laminate ME composite due to the plane-stress condition, that is, the resultant internal stress is zero along the layer thickness direction (z axis) and thus only the in-plane bias stress is produced in the laminate composite. In this work, the poling-generated bias strain in the PZT layer is treated explicitly through polarization domain evolution during simulated poling procedure, while the remaining part of the bias strain is treated in terms of an in-plane bias strain ε in the Terfenol-D layer. To systematically study the strain effect on magnetic susceptibility and its tunability, various magnitudes of the bias strain ε are considered in the computer simulations and for each ε, tunable electric field within a specific range is applied.

To simulate the magnetic susceptibility of Terfenol-D/PZT ME composites, the same following procedure is adopted in all simulation cases. Firstly, the in-plane (x-y plane) bias strain ε of a given value is exerted on the PZT layer. Secondly, a strong out-of-plane (z-axis) electric field is applied on the PZT layer for a full electrical poling, after which the ferroelectric domains are fully relaxed upon removal of the poling field. Thirdly, a series of electric field within a certain tuning range is applied perpendicular to the PZT layer to induce a tunable stress on Terfenol-D layer via strain-coupling effect. Finally,

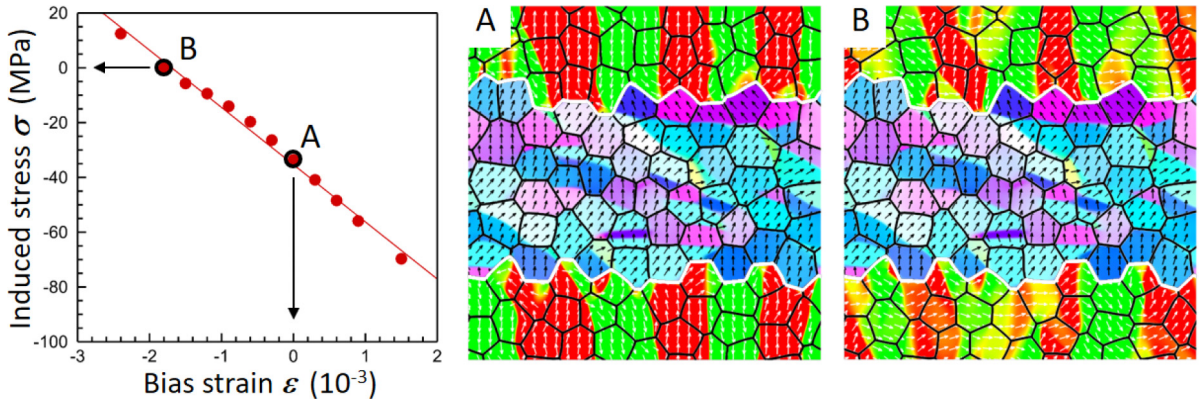

FIG. 2. In-plane stress σ in Terfenol-D layer induced by bias strain ε in PZT layer, and resultant domain structures of PZT and Terfenol-D layers at points A and B, which correspond to zero bias strain ($\varepsilon = 0$) and zero induced stress ($\sigma = 0$), respectively. Black and white arrows represent polarization and magnetization vectors, respectively. To distinguish the composite structure, polarization domain structure in PZT layer is visualized by color map with red, green, blue (RGB) components proportional to P_x, P_y, P_z, and magnetic domain structure in Terfenol-D layer is visualized by color contour proportional to M_z.

a small magnetic field ΔH along the y axis is applied on the Terfenol-D layer to induce a small magnetization response ΔM, from which the simulated magnetic susceptibility can be obtained by $\chi = \Delta M/\Delta H$.

In this systematical study, a series of internal bias strain ε from -2.4×10^{-3} to 1.5×10^{-3} is exerted in the PZT layer, which will induce a stress in the Terfenol-D layer. Since electrical poling of the PZT layer also exerts a stress on the Terfenol-D layer, the total stress that determines initial magnetic domain structures and initial susceptibility magnitudes should include both contributions. Figure 2 shows the total induced stress σ in the Terfenol-D layer as a function of the bias strain ε in the PZT layer, which, as expected, exhibits a linear interdependence within a certain range of the bias strain. It is worth noting that there are two points of particular interest in Fig. 2: point A with zero bias strain ($\varepsilon = 0$) and point B with zero induced stress ($\sigma = 0$). Point A of zero bias strain corresponds to a ME composite where the unpoled PZT layer is bonded with the Terfenol-D layer and subsequently poled; thus, a compressive stress is generated in the Terfenol-D layer caused by the poling procedure, while point B of zero induced stress corresponds to a ME composite where the PZT layer is poled before bonded with the Terfenol-D layer, thus no internal stress is generated. According to the simulation results, the poling generates a bias strain of -1.8×10^{-3} in the PZT layer, and thus use of a bias strain $\varepsilon = -1.8 \times 10^{-3}$ in the Terfenol-D layer can completely cancel the in-plane stress induced by electrical poling of the PZT layer, leading to point B in Fig. 2. Domain structures of ME composites corresponding to points A and B are also shown in Fig. 2. As expected for the electrically poled PZT layer, almost all polarization vectors point toward the poling direction (positive z axis) corresponding to both points A and B. However, the magnetic domain structure manifests a big difference: corresponding to point A, almost all magnetization vectors are oriented along positive or negative z axis forming 180° domain walls due to the stress-induced uniaxial anisotropy, while corresponding to point B, the magnetization vectors are oriented with significant components within the x-y plane due to lack of stress-induced anisotropy and large demagnetization field. Starting from those initial domain structures, once a tunable electric field is applied, the domain evolution takes place and hence the magnetic susceptibility is tuned. Figure 3 and Fig. 4 show the respective simulated results for case A and case B (starting from points A and B, respectively). Since the domain structure of poled PZT layer does not change significantly with the tuning electric field, hereafter only the magnetic domain structures of the Terfenol-D layer are visualized for clarity.

Under zero internal bias strain ($\varepsilon = 0$), the electrical poling of the PZT layer induces an in-plane compressive stress (−36 MPa) on the Terfenol-D layer, which is equivalent to a large magnetic uniaxial anisotropy with the easy axis perpendicular to the layer (i.e., along the z axis). Such a large stress-induced anisotropy leads to the out-of-plane alignment of magnetization vectors and the formation of multiple antiparallel domains in the Terfenol-D layer, as shown in Fig. 3(b). To simulate the susceptibility, a small magnetic field $\Delta H = 3$ Oe along the y axis is applied which induces a small magnetization response ΔM in the same direction. The simulated susceptibility is $\chi = \Delta M/\Delta H = 8.2$ for the ME composite at $E = 0$ under zero bias strain. Since the small magnetic field is almost perpendicular to all magnetic domains and domain walls, the obtained susceptibility is mainly contributed by the domain-rotation process rather than the domain-wall motion process. When an electric field is applied, the susceptibility is tuned due to the change in the stress-induced anisotropy. Figure 3(a) shows the simulated susceptibility as a function of the tunable electric field. As the electric field is tuned from $E = -15$ to 40 kV/cm, the susceptibility decreases from $\chi = 10.0$ to 4.8. Actually, such a decrease in susceptibility arises from the increased compressive stress ($\sigma = -28 \rightarrow -57$ MPa) and the resultant increased stress-induced anisotropy. Larger anisotropy makes the magnetization rotation more difficult and thus reduces the susceptibility. However, larger electric field or stress-induced anisotropy does not change the domain structure significantly, and only better align the magnetization vectors along the z axis, as shown in Fig. 3(c) at $E = 40$ kV/cm. Note that the susceptibility almost changes linearly with electric field

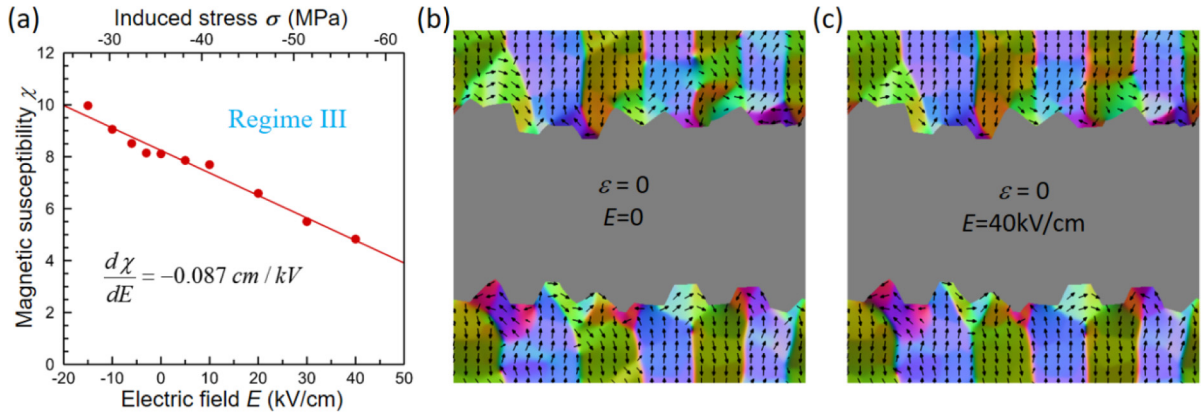

FIG. 3. (a) Simulated magnetic susceptibility χ as a function of electric field E (or induced stress σ) for Terfenol-D/PZT ME composites under zero internal bias strain ($\varepsilon = 0$). Red line represents linear fitting curve with slope $d\chi/dE = -0.087$ cm/kV. Magnetic domain structures of Terfenol-D layer under (b) $E = 0$ kV/cm and (c) $E = 40$ kV/cm. Black arrows represent magnetization vectors. Magnetic domain structures are visualized by color map with RGB components proportional to M_x, M_y, M_z.

in this range of tuning electric field with a slope of $d\chi/dE = -0.087$ cm/kV as shown in Fig. 3(a). As will be discussed later, such a nearly linear χ-E relation with a negative slope $d\chi/dE$ is characteristic of the magnetic susceptibility behavior in regime III.

ME composites under zero internal bias stress ($\sigma = 0$ achieved with internal bias strain $\varepsilon = -1.8 \times 10^{-3}$ as discussed above) manifest quite different susceptibility and domain behaviors from the above case. Due to the absence of stress-induced anisotropy, the demagnetization field effect prefers the magnetization vectors to stay in the x-y plane, as shown in Fig. 4(b). Since the demagnetization field is not uniform due to varying domain structures and uneven layer interfaces, the intrinsic magnetocrystalline anisotropy of the grains competes against the inhomogeneous demagnetization field and thus makes the in-plane magnetization alignment imperfect, and some magnetization vectors orient partially out of plane. At zero electric field, the susceptibility is $\chi = 2.8$, and such a small value actually results from the mostly in-plane domain structure. Figure 4(a) shows the simulated susceptibility as a function of tunable electric field. As the electric field is tuned from $E = -20$ to 40 kV/cm, the susceptibility increases from 2.52 to 4.80, with an average slope of $d\chi/dE = 0.037$ cm/kV, which is positive in contrast to the case of zero bias strain shown in Fig. 3. In this case, increasing the electric field leads to an increased compressive stress ($\sigma = 7 \rightarrow -12$ MPa) and thus an increased stress-induced anisotropy in the Terfenol-D layer, which results in progressively more out-of-plane magnetization alignment to enhance the domain-rotation process and gradually increased susceptibility. Figure 4(c) shows the corresponding domain structure at $E = 40$ kV/cm with more out-of-plane magnetizations. A closer inspection of the χ-E relation shown in Fig. 4(a) reveals that the simulated susceptibility indeed falls into two different regimes: regime I for $E < 10$ kV/cm (or $\sigma > -3$ MPa), where the magnetizations mostly stay in the x-y plane and further reducing the electric field does not significantly change the domain structure and the susceptibility; and regime II for $E > 10$ kV/cm (or $\sigma < -3$ MPa), where further increasing the electric field gives rise to more out-of-plane magnetizations and thus effectively increases the susceptibility. While both regime I and II are characterized by positive slope $d\chi/dE$ in contrast to the negative slope $d\chi/dE$ in regime III, the susceptibility in regime I is relatively insensitive to the

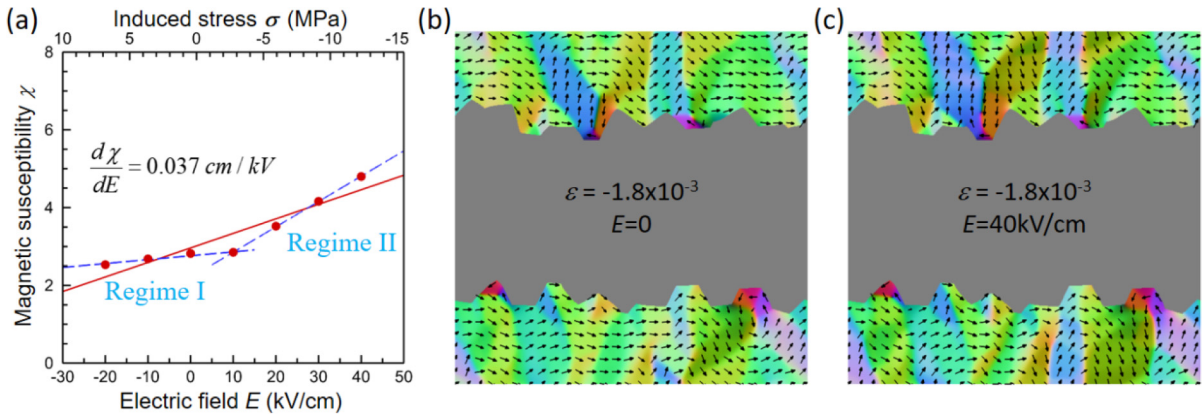

FIG. 4. (a) Simulated magnetic susceptibility χ as a function of electric field E (or induced stress σ) for Terfenol-D/PZT ME composites under zero internal bias stress ($\sigma = 0$). Red line represents linear fitting curve with slope $d\chi/dE = 0.037$ cm/kV. Blue dashed lines represent the linear fitting in regimes I and II. Magnetic domain structure of Terfenol-D layer under (b) $E = 0$ kV/cm and (c) $E = 40$ kV/cm.

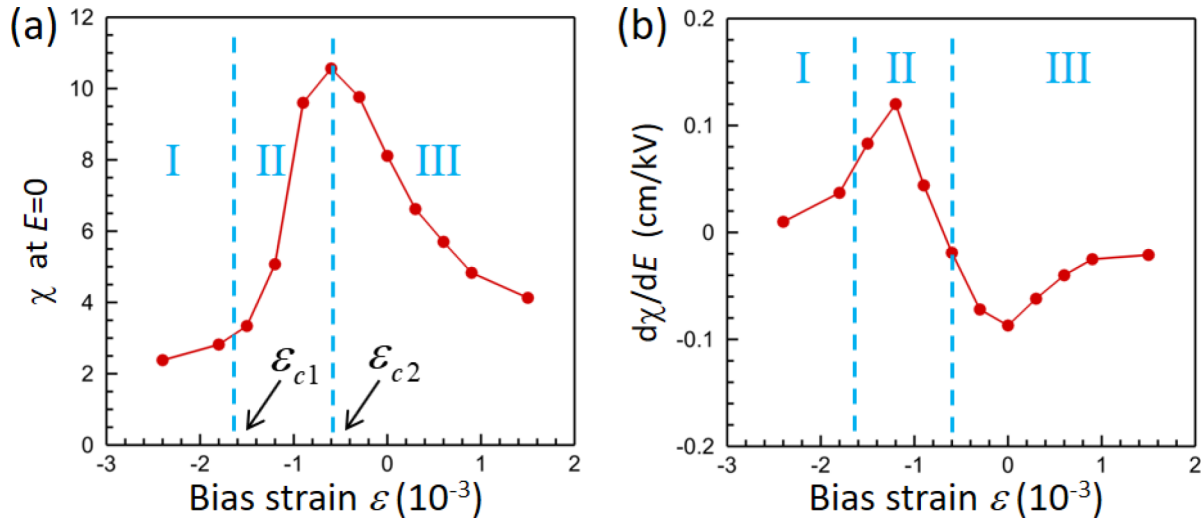

FIG. 5. (a) Simulated susceptibility χ at $E = 0$ as a function of bias strain ε from -2.4 to 1.5×10^{-3}. Three susceptibility regimes (I, II, and III) are divided by two critical bias strain values, $\varepsilon_{c1} \approx -1.6 \times 10^{-3}$ and $\varepsilon_{c2} \approx -0.6 \times 10^{-3}$. (b) The linear fitting slope $d\chi/dE$ as a function of bias strain ε in the three regimes.

tuning electric field (for instance, the χ-E slope in regime II is about 6 times that in regime I). Further increasing electric field beyond regime II will induce greater compressive stress and greater out-of-plane anisotropy, resulting in decreased susceptibility, entering regime III as discussed above.

While different domain structures and susceptibility behaviors are demonstrated for the two specific cases shown in Fig. 3 and Fig. 4, to investigate the whole-range susceptibility and tunability behaviors of the ME composite, more cases with different internal bias strain magnitudes are systematically simulated. For each case with a given bias strain, tunable electric field is applied to simulate the magnetic susceptibility and its tunability. Figure 5(a) shows the simulated susceptibility at $E = 0$ as a function of bias strain ε within the range of -2.4 to 1.5×10^{-3}. Note that the magnetic susceptibility reaches its maximum at $\varepsilon = -0.6 \times 10^{-3}$, while deviation from such a critical bias strain leads to continuous decrease in susceptibility. According to the domain structures and susceptibility behaviors discussed above for the two specific cases shown in Fig. 3 and Fig. 4, three regimes can be defined for the simulated susceptibility behavior and each regime is dominated by a different mechanism. Regime I and regime II are divided by $\varepsilon_{c1} \approx -1.6 \times 10^{-3}$ corresponding to $E = 10$ kV/cm or $\sigma = -3$ MPa in Fig. 4(a), while regime II and regime III are divided by $\varepsilon_{c2} \approx -0.6 \times 10^{-3}$ corresponding to the magnetic susceptibility maximum, as shown in Fig. 5(a). In regime I, almost all the magnetization vectors in the Terfenol-D layer lie in the x-y plane, and decreasing the bias strain does not increase the in-plane magnetization alignment, leading to small susceptibility and small tunability. In regime II, increasing the bias strain increases the compressive bias stress, leading to more out-of-plane magnetization alignment and increased susceptibility. It is worth noting that regime II is quite narrow, in which domain structures are sensitive to the bias strain, internal stress, and tuning electric field, leading to fast-increasing susceptibility and hence large tunability. In regime III, almost all the magnetization vectors are aligned out of plane, and increasing the bias strain and compressive stress makes magnetization rotation more difficult, leading to decreased susceptibility.

As mentioned above, the induced stress exerted on the Terfenol-D layer produces a uniaxial anisotropy along the z axis, which controls the magnetic domain structure and susceptibility. Figure 6 shows three representative magnetic domain structures under different bias strain to illustrate the stress-induced domain evolution process. Figure 6(a) corresponds to a tension stress exerted on the Terfenol-D layer, where most magnetization vectors lie in the x-y plane due to the stress-induced negative uniaxial anisotropy. Figure 6(b) illustrates the domain structure caused by a compressive stress and the resultant positive uniaxial anisotropy, where antiparallel domains start to form with most magnetization vectors aligned out of plane, corresponding to the maximum magnetic susceptibility at $\varepsilon = -0.6 \times 10^{-3}$ shown in Fig. 5(a). Figure 6(c) shows the domain structure under a large compressive stress, where almost all magnetization vectors are already aligned out of plane, and thus further increasing the stress-induced anisotropy does not significantly change the domain structure.

According to Fig. 5(a), large tunability can be predicted to occur in regimes II and III rather than regime I. Figure 5(b) shows the χ-E slopes to characterize the tunability as a function of bias strain ε. As expected, two tunability peaks emerge: one at $\varepsilon = -1.2 \times 10^{-3}$ in regime II with a positive slope of 0.120 kV/cm, while the other at $\varepsilon = 0$ in regime III with a negative slope of -0.087 kV/cm. It is worth noting that the latter in regime III just corresponds to the aforementioned case with zero bias strain shown in Fig. 3, while the former in regime II exhibits an even greater tunability. To reveal more details of the former case with $\varepsilon = -1.2 \times 10^{-3}$, Fig. 7 shows the simulated susceptibility and the corresponding domain structures. At zero electric field, the susceptibility is $\chi = 5.0$. Figure 7(a) shows the simulated susceptibility as a function of tunable electric field. As the electric field increases from $E = -20$ to 40 kV/cm, the compressive stress is tuned from $\sigma = -5$ to -22 MPa, which falls in regime II and exhibits the

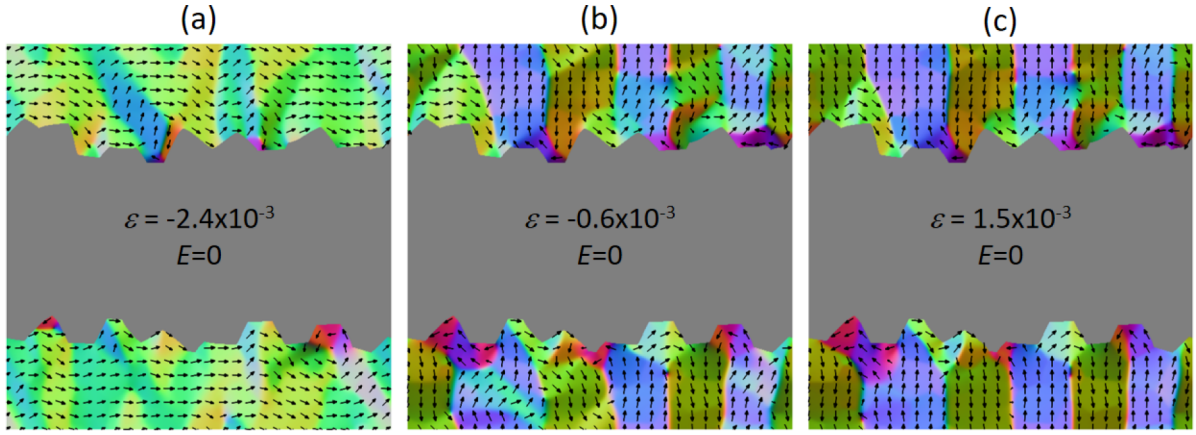

FIG. 6. Magnetic domain structures of Terfenol-D layer under representative bias strain of (a) $\varepsilon = -2.4 \times 10^{-3}$, (b) -0.6×10^{-3}, and (c) 1.5×10^{-3}.

largest tunability. Within this tuning range, the susceptibility increases from 3.2 to 9.6 with a positive slope of $d\chi/dE = 0.120$ cm/kV, which is much larger than any other case, and such a large tunability is attributed to the stress-sensitive domain structures. When the stress-induced anisotropy on the Terfenol-D layer is continuously increased, more out-of-plane magnetization alignment is induced that enhances the domain-rotation process, as shown in Figs. 7(b) and 7(c), effectively increasing the susceptibility and eventually producing a large tunability. Although the above-simulated results and discussions are based on the ME composites that utilize Terfenol-D as the magnetostrictive inductor material, the general behaviors of susceptibility and tunability revealed by this study are also applicable to ME inductors made of other polycrystalline magnetostrictive materials.

IV. THEORETICAL MODEL

To further characterize the simulated susceptibility behaviors of the laminate Terfenol-D/PZT ME composites discussed in Sec. III, a general theoretical model is developed based on the underlying domain-level mechanisms revealed in the above computer simulations. Although a few models have been proposed to study the stress-dependent magnetic susceptibility [22–24], they mainly focus on amorphous magnetostrictive materials in traditional inductors, thus a theoretical model treating polycrystalline magnetostrictive materials in VTIs is still lacking. In this section, we propose a theoretical model that takes into account the magnetocrystalline anisotropy in randomly oriented polycrystal grains and describes the interplay between effective magnetocrystalline anisotropy and stress-induced anisotropy as well as the resultant susceptibility behaviors of Terfenol-D/PZT ME composites over the three regimes. It also provides a general understanding of the stress-modulated susceptibility behaviors exhibited by VTIs built from different polycrystalline magnetostrictive materials.

In this theoretical model, the magnetization direction is described by $\mathbf{M} = M_s(\sin\theta\cos\varphi, \sin\theta\sin\varphi, \cos\theta)$, as illustrated in Fig. 8(a). For polycrystalline magnetostrictive materials, a unit vector $\mathbf{p} = (\sin\theta_0\cos\varphi_0, \sin\theta_0\sin\varphi_0, \cos\theta_0)$ characterizes the local magnetization easy axis that is closest to the magnetization direction $\mathbf{m} = \mathbf{M}/M_s = (\sin\theta\cos\varphi, \sin\theta\sin\varphi, \cos\theta)$ in a grain. The magnetocrystalline anisotropy energy in Eq. (2) can be approximately expanded around the easy axis $\mathbf{p}$ in a form of uniaxial

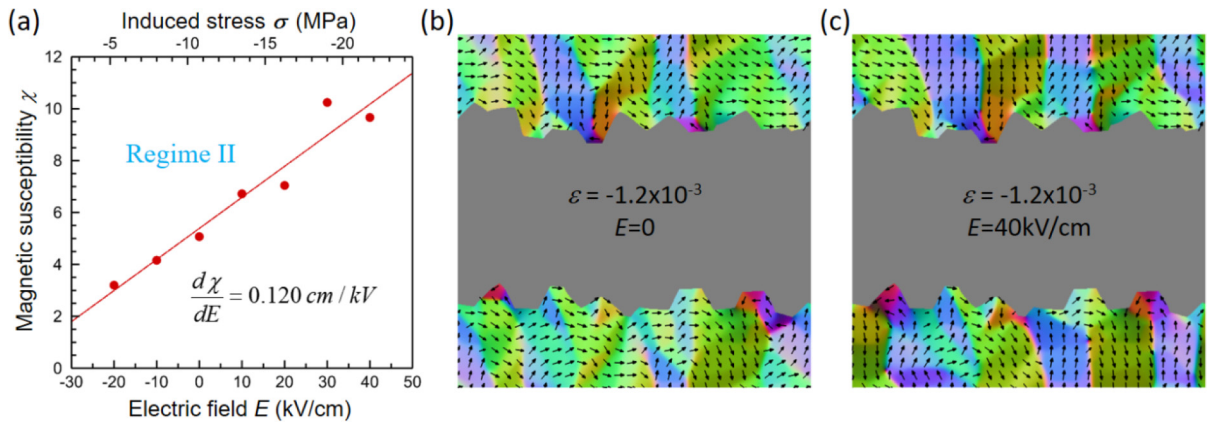

FIG. 7. (a) Simulated magnetic susceptibility χ as a function of electric field E (or induced stress σ) for Terfenol-D/PZT ME composites under internal bias strain $\varepsilon = -1.2 \times 10^{-3}$. Red line represents linear fitting curve with slope $d\chi/dE = 0.120$ cm/kV. Magnetic domain structures of Terfenol-D layer under (b) $E = 0$ kV/cm and (c) $E = 40$ kV/cm.

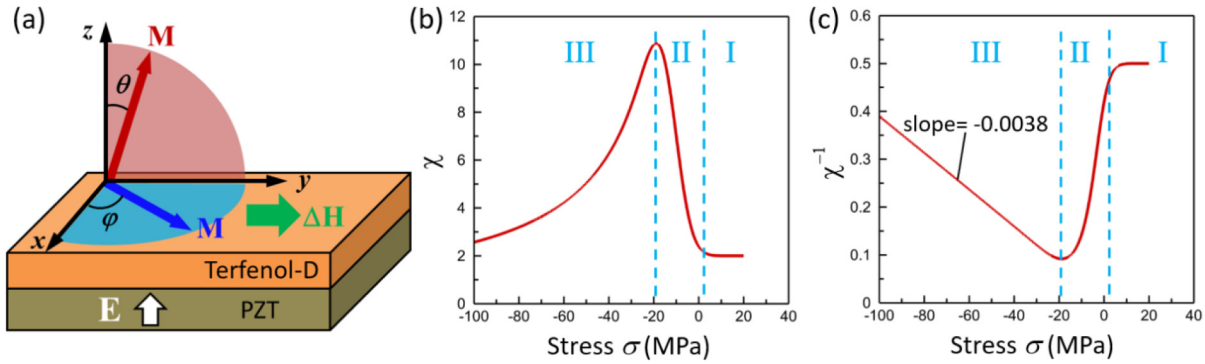

FIG. 8. (a) Schematic illustration of laminate ME composite and coordinate system. Calculated (b) susceptibility χ and (c) χ^{-1} as a function of stress σ based on the theoretical model for polycrystalline magnetostrictive materials.

anisotropy $f_M = K_0[1-(\mathbf{m}\cdot\mathbf{p})^2]$, where $K_0 = -\frac{2}{3}K_1 - \frac{2}{9}K_2$ ($K_0 = 8.44\times10^4$ J/m^3 for Terfenol-D). The effective magnetocrystalline anisotropy in the polycrystal will be obtained by averaging over θ_0 and φ_0 for randomly distributed grain orientations. In addition to the effective magnetocrystalline anisotropy, the magnetic domain structure and susceptibility in a laminate ME composite system are also controlled by stress-induced anisotropy and shape anisotropy. The stress-induced anisotropy is characterized by an energy term $K_\sigma = -\frac{3}{2}\lambda_s[\sigma_{xx}(m_x^2-\frac{1}{3})+\sigma_{yy}(m_y^2-\frac{1}{3})]$, where $\lambda_s = \frac{3}{5}\lambda_{111}+\frac{2}{5}\lambda_{100}$ is saturation magnetostriction constant ($\lambda_s = 1.0\times10^{-3}$ for Terfenol-D), and σ_{xx} and σ_{yy} are the in-plane stress components from both internal bias stress and tunable stress induced by electric field. The shape anisotropy is described by demagnetization energy term in the magnetostrictive layer, which depends on the magnetic domain structure and thus its magnitude is usually significantly smaller than $K_{d0} = 0.5\,\mu_0 M_s^2$ [26]. It is the competition between these three anisotropy terms that determines the susceptibility behavior. As revealed in above computer simulations, in regime I under large tensile stress where a negative K_σ dominates, the magnetization vector lies inside the x-y plane ($\theta\to\pi/2$); on the other hand, in regime III under large compressive stress where a positive K_σ dominates, the magnetization vector lies out of the x-y plane along the stress-induced easy z axis ($\theta\to 0$ or π). Between regime I and III, there exists a transition regime II, whose range is determined by the inhomogeneous domain structures and the resultant demagnetization energy K_d as well as the effective magnetocrystalline anisotropy, which usually leads to a sharp increase in susceptibility as the compressive stress increases and thus yields a large tunability.

Based on above simplifying assumptions, the total free energy under induced in-plane stress σ and small external magnetic field ΔH applied along the y axis is given by

$$F = K_0[1-(\mathbf{m}\cdot\mathbf{p})^2] + K_d m_z^2 - \frac{3}{2}\lambda_s\left[\sigma_{xx}\left(m_x^2-\frac{1}{3}\right) + \sigma_{yy}\left(m_y^2-\frac{1}{3}\right)\right] - \mu_0 M_s \Delta H m_y. \quad (9)$$

The second term is the demagnetization energy, where K_d is usually much smaller than the maximum value $K_{d0} = 0.5\,\mu_0 M_s^2$ as discussed above. For a magnetostrictive layer of in-plane dimensions much greater than its thickness, the in-plane components of induced stress are equiaxial $\sigma_{xx} = \sigma_{yy} = \sigma$. As such, Eq. (9) can be reformulated as

$$F = K_0[1-(\sin\theta\cos\varphi\sin\theta_0\cos\varphi_0 + \sin\theta\sin\varphi\sin\theta_0\sin\varphi_0 + \cos\theta\cos\theta_0)^2] + (K_d - K_\sigma)\cos^2\theta + \tfrac{1}{3}K_\sigma - \mu_0 M_s\Delta H\sin\theta\sin\varphi, \quad (10)$$

where $K_\sigma = -3\lambda_s\sigma/2$ is the stress-induced anisotropy (note that $\sigma<0$ for compressive stress).

In regime I under large tensile stress, a negative K_σ dominates so that the magnetization vector lies inside the x-y plane ($\theta=\pi/2$), and Eq. (10) becomes

$$F_I = K_0[1-\sin^2\theta_0\cos^2(\varphi-\varphi_0)] + \tfrac{1}{3}K_\sigma - \mu_0 M_s\Delta H\sin\varphi. \quad (11)$$

Since the magnetization vector stays close to the direction of easy axis $\mathbf{p}$, $\varphi-\varphi_0 = \Delta\varphi$ is a small angle. Solving $\partial F_I/\partial\Delta\varphi = 0$ gives magnetization response ΔM to magnetic field ΔH, yielding the magnetic susceptibility $\chi_I(\theta_0,\varphi_0) = dM/dH$ as

$$\chi_I(\theta_0,\varphi_0) = \frac{\mu_0 M_s^2\cos^2\varphi_0}{2K_0\sin^2\theta_0}, \quad (12)$$

which depends on the direction of the easy axis $\mathbf{p}$ as specified by θ_0 and φ_0 in each grain. Upon orientation average over $\theta_0\in(\Psi,\pi-\Psi)$ and $\varphi_0\in(-\pi,\pi)$ for randomly oriented $\langle111\rangle$ easy axes in polycrystalline Terfenol-D, where $\Psi = \sin^{-1}(1/\sqrt{3})$, the effective susceptibility in regime I becomes

$$\chi_I = \langle\chi_I(\theta_0,\varphi_0)\rangle = \frac{\mu_0 M_s^2}{4K_I}, \quad (13)$$

where $\langle\cos^2\varphi_0\rangle = 1/2$, and $K_I = K_0\langle\sin^2\theta_0\rangle = K_0[1+\sin 2\Psi/(\pi-2\Psi)]/2 = 0.75K_0 = 6.3\times10^4$ J/m^3 is the effective magnetocrystalline anisotropy in regime I. Equation (13) shows that the effective susceptibility in regime I is a constant that depends only on the effective magnetocrystalline anisotropy K_I.

In regime III under large compressive stress, a positive K_σ dominates so that the magnetization vector lies out of the x-y plane along the stress-induced easy z axis ($\theta=0$ or π, which are equivalent with respect to the magnetic field ΔH applied along the y axis; for convenience, $\theta=0$ is considered). While φ is undefined in such a "ground state" of

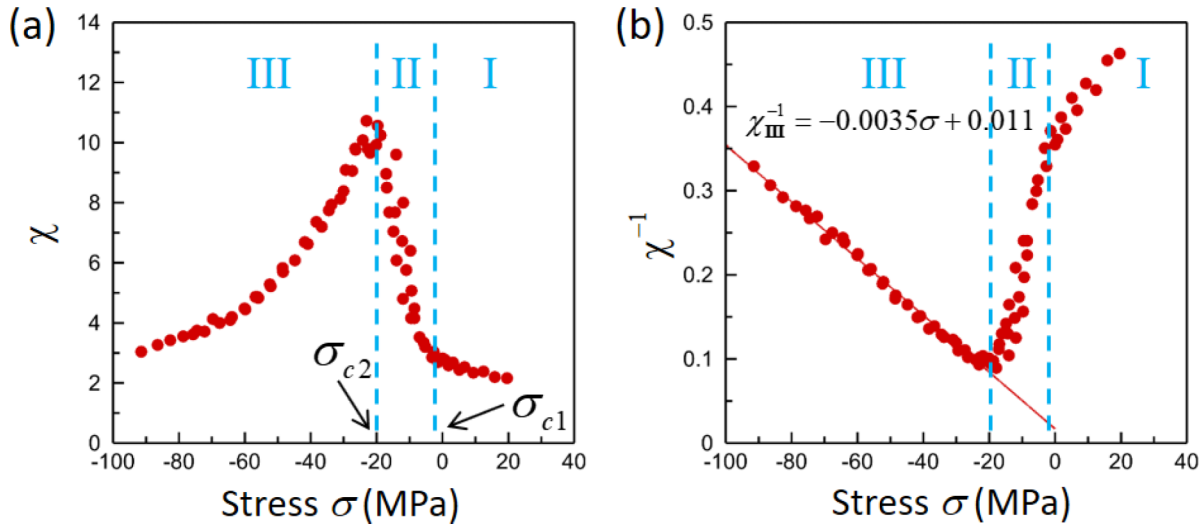

FIG. 9. (a) Simulated magnetic susceptibility χ as a function of induced stress σ. Three susceptibility regimes (I, II, and III) are defined by two critical induced stress values, $\sigma_{c1} \approx -3$ MPa and $\sigma_{c2} \approx -20$ MPa. (b) Plot of χ^{-1} as a function of induced stress σ. Red line represents linear fitting in regime III: $\chi_{\rm III}^{-1} = -0.0035\sigma + 0.011$.

regime III, application of magnetic field ΔH along the y axis induces magnetization response ΔM in the same direction, thus θ is a small angle and $\varphi = \pi/2$ can be assumed under ΔH, and Eq. (10) becomes

$$F_{\rm III} = K_0[1 - (\sin\theta\sin\theta_0\sin\varphi_0 + \cos\theta\cos\theta_0)^2] + (K_d - K_\sigma)\cos^2\theta + \tfrac{1}{3}K_\sigma - \mu_0 M_s \Delta H \sin\theta. \quad (14)$$

Solving $\partial F_{\rm III}/\partial\theta = 0$ gives magnetization response ΔM to magnetic field ΔH, yielding the magnetic susceptibility $\chi_{\rm III}(\theta_0, \varphi_0) = dM/dH$ as

$$\chi_{\rm III}(\theta_0, \varphi_0) = \frac{\mu_0 M_s^2}{2K_0(\cos^2\theta_0 - \sin^2\theta_0\sin^2\varphi_0) - 2(K_d - K_\sigma)}, \quad (15)$$

which depends on the direction of the easy axis **p** as specified by θ_0 and φ_0 in each grain. Upon orientation average over $\theta_0 \in (0, \Theta)$ and $\varphi_0 \in (-\pi, \pi)$ for randomly oriented $\langle 111\rangle$ easy axes in polycrystalline Terfenol-D, where $\Theta = \sin^{-1}(\sqrt{2}/\sqrt{3})$, the effective susceptibility in Regime III becomes

$$\chi_{\rm III} = \langle\chi_{\rm III}(\theta_0, \varphi_0)\rangle = \frac{\mu_0 M_s^2}{2(K_{\rm III} - K_d + K_\sigma)}, \quad (16)$$

where $\langle\cos^2\theta_0\rangle = 1/2 + \sin 2\Theta/4\Theta = 0.75$, $\langle\sin^2\theta_0\rangle = 1/2 - \sin 2\Theta/4\Theta = 0.25$, $\langle\sin^2\varphi_0\rangle = 1/2$, and $K_{\rm III} = K_0(\langle\cos^2\theta_0\rangle - \langle\sin^2\theta_0\rangle\langle\sin^2\varphi_0\rangle) = 0.62K_0 = 5.2 \times 10^4$ J/m^3 is the effective magnetocrystalline anisotropy in regime III. It is worth noting that Eq. (16) reveals a linear relationship between the reciprocal susceptibility $\chi_{\rm III}^{-1}$ and stress σ in regime III, which is more evident upon reformulation:

$$\chi_{\rm III}^{-1} = \frac{2(K_{\rm III} - K_d)}{\mu_0 M_s^2} - \frac{3\lambda_s}{\mu_0 M_s^2}\sigma. \quad (17)$$

Therefore, it is expected that a large tunability with a desirable linear dependence on tuning stress (and voltage) can be achieved in regime III if the stress is tuned in a large range.

To compare the theoretical predictions and the simulation results, the data points of the phase-field simulated susceptibility χ and its reciprocal χ^{-1} are plotted as a function of stress σ over the three regimes in Fig. 9. Figure 9(a) shows $\chi_I \approx 2$ in regime I, which according to Eq. (13) corresponds to an effective magnetocrystalline anisotropy $K_I \approx 1.0 \times 10^5$ J/m^3. This value is about 60% greater than the theoretical value $K_I = 6.3 \times 10^4$ J/m^3. This discrepancy is attributed to three major factors: (1) the uniaxial crystallographic anisotropy approximation adopted in the theoretical model is accurate only for magnetization direction close to the easy axis while in regimes I and III the deviation angle of local magnetization vectors from easy axes in some grains may be not small due to random grain orientations; (2) the orientation averaging procedure performed in Eqs. (13) and (16) treats θ_0 and φ_0 as uniformly distributed in respective ranges while such simplification does not accurately describe random grain orientation distribution with uniform probability; and (3) the phase-field simulation considers only a finite number of grains in the Terfenol-D layer which is insufficient to sample random grain orientation. Despite these theoretical simplifications and computational limitations, the obtained values of the effective magnetocrystalline anisotropy K_I in regime I are of the same order of magnitude, indicating that the theoretical model captures the main mechanisms of magnetic susceptibility behavior. Figure 9(b) shows a linear relationship of $\chi^{-1} \sim \sigma$ in regime III with a slope -0.0035 MPa^{-1}, in good agreement with the theoretical slope $-3\lambda_s/\mu_0 M_s^2 = -0.0038$ MPa^{-1} according to Eq. (17). Also, according to Eq. (17) and Fig. 9(b), $2(K_{\rm III} - K_d)/\mu_0 M_s^2 = 0.011$ gives $K_{\rm III} - K_d = 4.4 \times 10^3$ J/m^3. Using $K_{\rm III} = 5.2 \times 10^4$ J/m^3 yields $K_d = 4.76 \times 10^4$ J/m^3, which is significantly smaller than $K_{d0} = 0.5\,\mu_0 M_s^2 = 4.02 \times 10^5$ J/m^3 as expected. It is worth noting that such a linear relationship $\chi^{-1} \sim \sigma$ was also observed in amorphous inductor materials when the stress is large enough to orient magnetization along the stress-induced easy axis [30–33].

Regime II is a smooth transition between regimes I and III, which is associated with the gradual reorientation of magnetization from in-plane alignment under tensile stress in regime I to out-of-plane alignment under compressive stress in regime III caused by the change in the stress. Figure 9(a)

plots the three regimes of the simulated susceptibility that are defined by two critical stress values, σ_{c1} and σ_{c2}. In contrast to regimes I and III, regime II is narrower and the susceptibility changes significantly, thus providing higher tunability per unit stress (or voltage). During the gradual reorientation of magnetization caused by the change in stress in regime II, the magnetic domain structure also gradually evolves as shown in Fig. 6, leading to change in the demagnetization energy K_d. To capture such an effect and reproduce the transition regime II, a Gaussian distribution of the demagnetization energy K_d around $K_d = 4.76 \times 10^4\,\mathrm{J/m^3}$ with a standard deviation $\sigma_K = 9 \times 10^3\,\mathrm{J/m^3}$ is assumed in the theoretical model. The susceptibility χ and χ^{-1} as a function of stress σ calculated from this theoretical model are plotted in Figs. 8(b) and 8(c), respectively, which show good agreement with the simulated results shown in Fig. 9. In regime I the susceptibility approaches a constant value $\chi_I \approx 2$, and in regime III the linear relationship between χ^{-1} and σ is reproduced with the theoretical slope consistent with the simulated one.

The effects of the domain-level mechanisms responsible for the three susceptibility regimes as revealed by the phase-field simulations are captured by above theoretical model of the polycrystalline Terfenol-D/PZT ME composites. This model predicts three susceptibility regimes, which is different from the previous model of amorphous Metglas/PZT ME composites [20] where only two susceptibility regimes exist due to different magnetic anisotropy. While the direct and converse ME effects in laminate Terfenol-D/PZT composites have been extensively studied [34–37], the electric field control of magnetic susceptibility in those Terfenol-D/PZT composites was much less investigated; nevertheless, the existence of regime III was experimentally evidenced by the observed stress-induced permeability behavior of Terfenol-D magnetostrictive transducers [38,39]. It is worth noting that similar susceptibility behaviors exist in other polycrystalline magnetostrictive inductor materials. For example, regime III is experimentally observed in VTIs made of cofired polycrystalline ferrite/PMN-PT ME composites [19], while regimes I and II are observed in bonded polycrystalline ferrite/PMN-PT ME composites [18,40]. Among the three regimes, large tunability can be achieved in either regime II or regime III. In regime III, the reciprocal susceptibility χ^{-1} changes linearly with stress σ, thus a large tunability can be obtained if the tuning range in stress is wide, which requires a large piezoelectric constant d_{31} and/or large dielectric breakdown strength for piezoelectric layer (a large magnetostriction coefficient λ_s for magnetostrictive layer is also desired). In regime II, the susceptibility changes significantly within a narrow tuning range, thus a high tunability could be achieved without the requirements for large piezoelectric constant, high dielectric breakdown strength, or large magnetostriction coefficient. It is worth noting that the tunability in regime II exhibits a strong dependency on the magnetocrystalline anisotropy, that is, a smaller magnetocrystalline anisotropy leads to a narrower regime II and a higher tunability per unit stress. As reported in our recent work for polycrystalline ferrite/PMN-PT VTIs [18,40], reducing the magnetocrystalline anisotropy effectively enhances the tunability in regime II and a colossal tunability up to 750% is obtained in VTIs with an almost diminished magnetocrystalline anisotropy.

V. CONCLUSION

Electric field control of magnetic susceptibility in laminate magnetostrictive/piezoelectric composites is of great importance in creating a new class of magnetoelectric elements, voltage tunable inductors. To elucidate the mechanism of electric field modulated magnetic susceptibility at the domain level, phase-field modeling and computer simulation are employed to systematically study the laminate Terfenol-D/PZT magnetoelectric composites. Polycrystalline Terfenol-D can provide a giant magnetoelectric coupling because of its large magnetostriction, which is important for high-tunability voltage tunable inductors. The simulations mainly focus on the interplay between magnetocrystalline anisotropy and stress-induced anisotropy. The stress-induced anisotropy is introduced by two types of strain, namely, electric field tunable strain and internal bias strain. The simulations reveal three regimes of magnetic susceptibility: Regime I corresponds to a nearly constant susceptibility, regime III exhibits a linear behavior of the reciprocal susceptibility, while regime II is a fast transition between regimes I and III. Actually, such three regimes are attributed to different magnetization distribution and evolution mechanisms that are modulated by the stress-induced anisotropy. The simulated results indicate that high tunability can occur in regime II or III. To further characterize the electric field control of magnetic susceptibility behaviors, a general theoretical model of laminate ME composites based on polycrystalline magnetostrictive materials is developed, which reproduces the three regimes of susceptibility behaviors for polycrystalline Terfenol-D material, in good agreement with the simulation findings. Such three regimes commonly exist in polycrystalline magnetostrictive inductor materials, such as in ferrite/PMN-PT ME composites [18,19,40]. This general theoretical model presented here for Terfenol-D model system can be also extended to other laminate magnetoelectric composites based on polycrystalline magnetostrictive materials.

ACKNOWLEDGMENTS

Financial support from DARPA MATRIX Program is acknowledged. The parallel computer simulations were performed on XSEDE supercomputers.

[1] J. Ma, J. Hu, Z. Li, and C.-W. Nan, Adv. Mater. **23**, 1062 (2011).
[2] C.-W. Nan, M. I. Bichurin, S. Dong, D. Viehland, and G. Srinivasan, J. Appl. Phys. **103**, 031101 (2008).
[3] Y. Wang, D. Gray, D. Berry, J. Gao, M. Li, J. Li, and D. Viehland, Adv. Mater. **23**, 4111 (2011).
[4] C.-W. Nan, Phys. Rev. B **50**, 6082 (1994).
[5] N. X. Sun and G. Srinivasan, SPIN **02**, 1240004 (2012).
[6] G. Sreenivasulu, S. K. Mandal, S. Bandekar, V. M. Petrov, and G. Srinivasan, Phys. Rev. B **84**, 144426 (2011).

[7] N. Cai, J. Zhai, C. W. Nan, Y. Lin, and Z. Shi, Phys. Rev. B **68**, 224103 (2003).

[8] S. K. Mandal, G. Sreenivasulu, V. M. Petrov, and G. Srinivasan, Phys. Rev. B **84**, 014432 (2011).

[9] G. Sreenivasulu, V. M. Petrov, L. Y. Fetisov, Y. K. Fetisov, and G. Srinivasan, Phys. Rev. B **86**, 214405 (2012).

[10] H. Palneedi, D. Maurya, L. D. Geng, H.-C. Song, G.-T. Hwang, M. Peddigari, V. Annapureddy, K. Song, Y. S. Oh, S.-C. Yang, Y. U. Wang, S. Priya, and J. Ryu, ACS Appl. Mater. Interfaces **10**, 11018 (2018).

[11] M. I. Bichurin, V. M. Petrov, and G. Srinivasan, Phys. Rev. B **68**, 054402 (2003).

[12] M. I. Bichurin, V. M. Petrov, and G. Srinivasan, J. Appl. Phys. **92**, 7681 (2002).

[13] V. M. Petrov, G. Srinivasan, M. I. Bichurin, and A. Gupta, Phys. Rev. B **75**, 224407 (2007).

[14] V. M. Petrov, G. Srinivasan, M. I. Bichurin, and T. A. Galkina, J. Appl. Phys. **105**, 063911 (2009).

[15] J. Lou, D. Reed, M. Liu, and N. X. Sun, Appl. Phys. Lett. **94**, 112508 (2009).

[16] G. Liu, X. Cui, and S. Dong, J. Appl. Phys. **108**, 094106 (2010).

[17] H. Lin, J. Lou, Y. Gao, R. Hasegawa, M. Liu, B. Howe, J. Jones, G. Brown, and N. X. Sun, IEEE Trans. Magn. **51**, 4002705 (2015).

[18] Y. Yan, L. D. Geng, Y. Tan, J. Ma, L. Zhang, M. Sanghadasa, K. Ngo, A. W. Ghosh, Y. U. Wang, and S. Priya, Nat. Commun. **9**, 4998 (2018).

[19] Y. Yan, L. D. Geng, L. Zhang, X. Gao, S. Gollapudi, H.-C. Song, S. Dong, M. Sanghadasa, K. Ngo, Y. U. Wang, and S. Priya, Sci. Rep. **7**, 16008 (2017).

[20] L. D. Geng, Y. Yan, S. Priya, and Y. U. Wang, Acta Mater. **140**, 97 (2017).

[21] Y. Y. Huang and Y. M. Jin, Appl. Phys. Lett. **93**, 142504 (2008).

[22] Y. U. Wang, J. Mater. Sci. **44**, 5225 (2009).

[23] F. D. Ma, Y. M. Jin, Y. U. Wang, S. L. Kampe, and S. Dong, Acta Mater. **70**, 45 (2014).

[24] A. E. Clark, J. P. Teter, and O. D. McMasters, J. Appl. Phys. **63**, 3910 (1988).

[25] A. Amin, M. J. Haun, B. Badger, H. McKinstry, and L. E. Cross, Ferroelectrics **65**, 107 (1985).

[26] A. Hubert and R. Schäfer, *Magnetic Domains: The Analysis of Magnetic Microstructures*, 1st ed. (Springer-Verlag, Berlin, 1998).

[27] S. Semenovskaya and A. G. Khachaturyan, J. Appl. Phys. **83**, 5125 (1998).

[28] Y. M. Jin, Appl. Phys. Lett. **103**, 021906 (2013).

[29] M. J. Haun, Z. Q. Zhuang, E. Furman, S. J. Jang, and L. E. Cross, J. Am. Ceram. Soc. **72**, 1140 (1989).

[30] G. Liu, Y. Zhang, P. Ci, and S. Dong, J. Appl. Phys. **114**, 064107 (2013).

[31] H. Chiriac and I. Ciobotaru, J. Magn. Magn. Mater. **124**, 277 (1993).

[32] H. T. Savage and M. L. Spano, J. Appl. Phys. **53**, 8092 (1982).

[33] M. L. Spano, K. B. Hathaway, and H. T. Savage, J. Appl. Phys. **53**, 2667 (1982).

[34] S. Dong, J. Cheng, J. F. Li, and D. Viehland, Appl. Phys. Lett. **83**, 4812 (2003).

[35] S. Dong, J. Zhai, J.-F. Li, and D. Viehland, Appl. Phys. Lett. **89**, 122903 (2006).

[36] P. Record, C. Popov, J. Fletcher, E. Abraham, Z. Huang, H. Chang, and R. W. Whatmore, Sens. Actuator B-Chem. **126**, 344 (2007).

[37] Y. P. Yao, Y. Hou, S. N. Dong, and X. G. Li, J. Appl. Phys. **110**, 014508 (2011).

[38] M. B. Moffett, J. M. Powers, and A. E. Clark, J. Acoust. Soc. Am. **90**, 1184 (1991).

[39] M. B. Moffett, A. E. Clark, M. Wun-Fogle, J. Linberg, J. P. Teter, and E. A. McLaughlin, J. Acoust. Soc. Am. **89**, 1448 (1991).

[40] L. D. Geng, Y. Yan, S. Priya, and Y. U. Wang, Acta Mater. **166**, 493 (2019).